2017

Structural Transformations in Diluted Micellar and Lamellar Systems

Blanca Zelaya-Rincón
University of Rhode Island, blanca.zelaya.rincon@gmail.com

STRUCTURAL TRANSFORMATIONS IN DILUTED MICELLAR AND LAMELLAR SYSTEMS

BY

BLANCA ZELAYA-RINCÓN

A THESIS SUBMITTED IN PARTIAL FULFILLMENT OF THE

REQUIREMENTS FOR THE DEGREE OF

MASTER OF SCIENCE

IN

CHEMICAL ENGINEERING

UNIVERSITY OF RHODE ISLAND

2017

MASTER OF SCIENCE

OF

BLANCA ZELAYA-RINCÓN

APPROVED:

Thesis Committee:

Major Professor Arijit Bose

Geoffrey Bothun

Sze Cheng Yang

Nasser H. Zawia
DEAN OF THE GRADUATE SCHOOL

UNIVERSITY OF RHODE ISLAND
2017

ABSTRACT

The role of dilution by artificial hard water on nanostructures present in body wash samples provided by Procter and Gamble were investigated using time-resolved cryogenic transmission electron microscopy (cryo-TEM). Samples with and without perfume were examined at 10X, 20X, and 50X dilution. Micellar samples transformed to mostly unilamellar vesicles at 50X dilution, in contrast to the micelle to monomer transition seen in typical samples. At lower dilutions, a change in morphology from spherical to wormlike micelles was observed. For lamellar samples, lower dilution ratios show tightly packed multilamellar vesicles, while higher dilution ratios show more dispersed vesicles with less bilayers. Nanostructural transformations upon dilution were attributed to changes in curvature/packing parameters, which occurred due to dilution with hard water and addition of perfume. The systems experience changes in curvature in order to maintain equilibrium. Also, the addition of perfume in the lamellar samples caused an increase in the number of bilayers present in multilamellar vesicles, because of its role in increasing the packing parameter in the system.

ACKNOWLEDGMENTS

Words are not enough to express my gratitude to my Major Professor, Arijit Bose, who has helped, supported, and guided me throughout the whole process.

Thank you to Procter and Gamble for providing the samples and financial support for this study. Thank you to Richard Kingsley at URI for providing cryo-TEM sample preparation and operation training, as well as for taking the images used in this study. Also, thank you to Yanjing Chen at URI for training/help with role transition given at the beginning of this study.

Additional thank you to Rosi Smith, Rebekah Gomez, Maria Liebhauser, and their families for all of the love and support.

Thank you to my mother's side of the family for always being by my side. Without all of your love, support, help, encouragement, and faith in me, I would not have been able to close this chapter in my life. Special thanks to my grandparents, my aunt Claudia, and my uncle Joel.

Finally, thank you to my mother who has always motivated my brother and me to do our best in life. Her strength, determination, and caring personality have inspired me to never give up.

TABLE OF CONTENTS

LIST OF TABLES

TABLE PAGE

LIST OF FIGURES

CHAPTER 1

INTRODUCTION

Body wash is an important consumer product. It consists of a complex mixture of surfactants and polymers, designed to produce rapid detergency action upon mixing with water and rubbing on skin, while providing the right feel for the user and being gentle on the skin [1, 2]. Its properties and performance are intimately related to the nanostructures present in the wash and changes to these nanostructures taking place because of dilution and mixing with water [1].

Micellar and lamellar systems can be found in many consumer products such as body wash, laundry detergent and shampoo [3]. These consumer product formulations often contain salts and perfume/raw materials, as well as different types of surfactants. There have been many studies focusing on the effects which the addition, removal, and change in concentration of these components have on these systems, as well as how shear affects the structures present in these systems [3-13]. Even so, there is still limited understanding as to how dilution affects the nanostructures present.

The skin barrier is a powerful film, made up of three major components: free fatty acids, ceramides, and cholesterol [14, 15]. A properly functioning skin barrier keeps out allergens, foreign materials, and reduces transepidermal water loss, therefore reducing skin dryness and irritation by keeping the balance between moisture and hydration, ultimately preventing skin diseases such as atopic dermatitis [15-17]. It is well known that certain surfactants such as SLS can be very harsh on the skin and actually strip the skin, meaning that although effective for cleansing all of the dirt and unwanted particles from skin, they also remove some of these major components of many of the skin barrier

[18]. This stripping of the skin barrier can cause slower skin regeneration after irritation occurs, and also makes penetration of foreign material and allergens easier, which can lead to conditions such as atopic dermatitis [16, 19]. Although there are now many gentler surfactants which are being studied and used, structural transformations in nanostructures present in these cleansing formulations can also have a drying effect, since it has been suggested that smaller nanostructures present in cleansing products tend to be more irritating to skin [19, 20].

This study focuses on the effects of dilution on the nanostructures present in micellar and lamellar systems. Specifically, the micellar and lamellar systems in this study are diluted with a salt solution (hard water), meaning that it may cause unexpected transformations to take place upon dilution [21]. However, there are many other factors which also need to be taken into consideration when diluting a system, such as mixing time, mixing method, whether or not perfume is present in the sample, and the sample preparation technique for cryogenic transmission electron microscopy (cryo-TEM).

Investigating what kinds of nanostructural transformations occur in different surfactant systems upon dilution with hard water, and using the results from this study in conjunction with previous knowledge regarding the maintenance of the skin barrier integrity, may be useful in the future optimization of body wash formulations, as well as cleansing formulations in general, to minimize skin irritation, dryness, and diseases such as atopic dermatitis.

CHAPTER 2

EXPERIMENTAL METHODS

Sample Preparation

Artificial hard water was made by adding 4.1 mg of calcium chloride dihydrate and 6.2 mg of magnesium chloride hexahydrate to 50 mL of DI water [22]. Total permanent water hardness was calculated by first calculating the concentration of Ca^{2+} and Mg^{2+} present in the DI water (in mg/L), since these are the prime cation contributors to water hardness [23]. These values were then expressed as equivalents of $CaCO_3$ and were added together to obtain a total hardness value [23]. The hard water used throughout this study was calculated to have a total hardness of 117 mg/L which is classified as moderately hard [24]. This method for making hard water in a laboratory is considered to be standard and was used because it most closely imitates the water people have access to in their homes [25].

The body wash samples were provided by Procter and Gamble. Samples of 10X dilution were made by mixing 300 microliters of original sample with 2700 microliters of hard water. Samples at 20X dilution were made by mixing 150 microliters of original sample with 2850 microliters of hard water, and samples at 50X dilution were made by mixing 60 microliters of original sample with 2940 microliters of hard water.

Sample Mixing

When body wash is used in the shower, a substantial amount of foam is produced with ease via dilution and scrubbing action. In order to mimic this production of foam samples were vortex mixed for 15 seconds, and then vitrified within 20 seconds after mixing. This mixing time of 15 seconds was chosen through personal experience and

inquiry about how long (on average) acquaintances spent using body wash while showering. Only the liquid layer was imaged.

The four original samples received from Procter and Gamble were: micellar no perfume (Mi), micellar with perfume (MiP), lamellar no perfume (La) and lamellar with perfume (LaP). Dilution will be indicated after these labels in order to indicate samples being referred to throughout this study (e.g. Mi10x would refer to the micellar sample with no perfume at 10x dilution).

Table 1. Chemical names and structures of surfactants and salt present in original samples received from Procter and Gamble.

Chemical Name	**Formula**	**Structure**	**Molecular Weight**	**Sample Presence**
Sodium Trideceth-2 Sulfate	$C_{19}H_{39}NaO_7S$ [26]	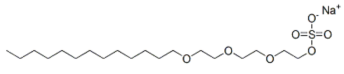 [26]	434.564	Mi, MiP, La, LaP
Cocamidopropyl Betaine	$C_{19}H_{38}N_2O_3$ [27]	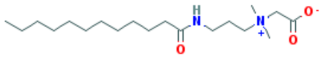 [27]	342.524	Mi, MiP, La, LaP
Trideceth-3	$C_{13}H_{27}(CH_2CH_2O)_3OH$	$C_{13}H_{27}$→branched hydrocarbon; approximately 2-3 methyl branches at random positions	332.525	La, LaP
Sodium Chloride	NaCl	Na^+—Cl^-	58.44	La, LaP

Note: Information for Trideceth-3 (formula and structure) given by Procter and Gamble

The table above shows the main/important components of the samples, which are mainly surfactants which were present. The chemical names were given by Procter and Gamble.

Cryogenic Transmission Electron Microscopy (cryo-TEM)

A blotless method was chosen for cryo-TEM sample preparation to avoid artifacts created by shear [28]. After pipetting the sample onto a holey carbon grid, excess liquid

was removed via syringe or capillary tube. The syringe (or capillary tube) was placed parallel to the plane of the grid as seen in the figure below.

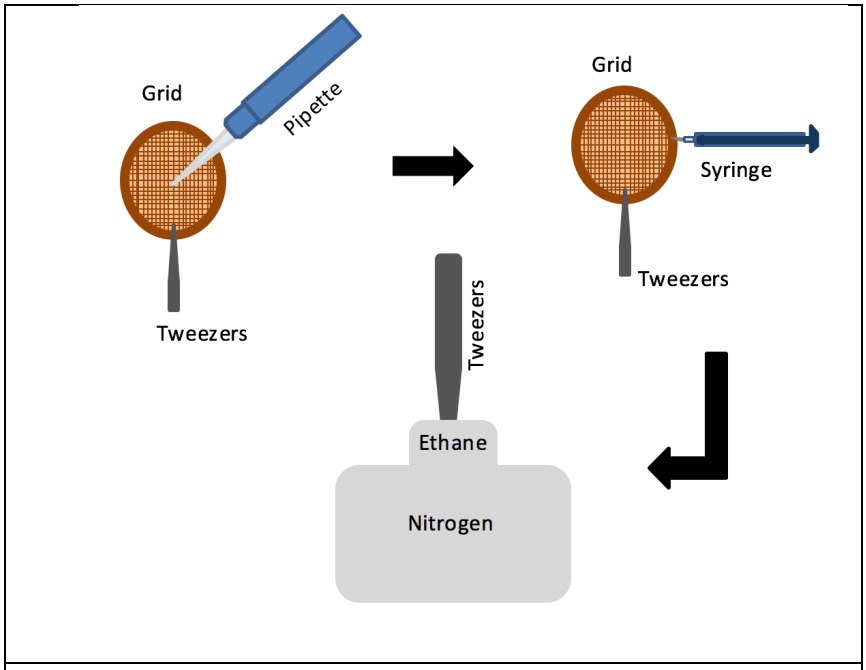

Figure 1. Blotless method schematic for cryo-TEM sample preparation

This geometry allowed sample to be thinned out without introducing any flow within the grid holes, therefore removing any shear-induced artifacts from the sample and images [28]. The sample was then vitrified in ethane and stored in a liquid nitrogen dewar until it was imaged. The grid was placed on a Gatan 626 DH cryo holder, inserted into a JEOL 2100 TEM. The sample's temperature was maintained at -165C during imaging.

Image Analysis

In order to estimate vesicle size (area in nm^2) ImageJ was used. The diameter of the vesicles was measured directly when round vesicles were present. However, for irregularly shaped vesicles the diameter had to be estimated in order to calculate the area as accurately as possible. The particle analysis functions were tested, but were not used

due to the complex nature of the systems imaged and low image contrast. Manual analysis proved to be the most effective choice for this study.

Results obtained through ImageJ analysis were averaged and the mean areas were plotted. Standard deviations are reported as error bars. They were also graphed as histograms. The outliers in the data were not included in the graphs, due to the fact their large values distorted the axis, making the smaller vesicle areas more difficult to visualize. However, they are included and highlighted in yellow in the Appendix.

CHAPTER 3

RESULTS AND DISCUSSION

Images of the micellar samples with and without perfume at the different dilutions are shown in Figure 2.

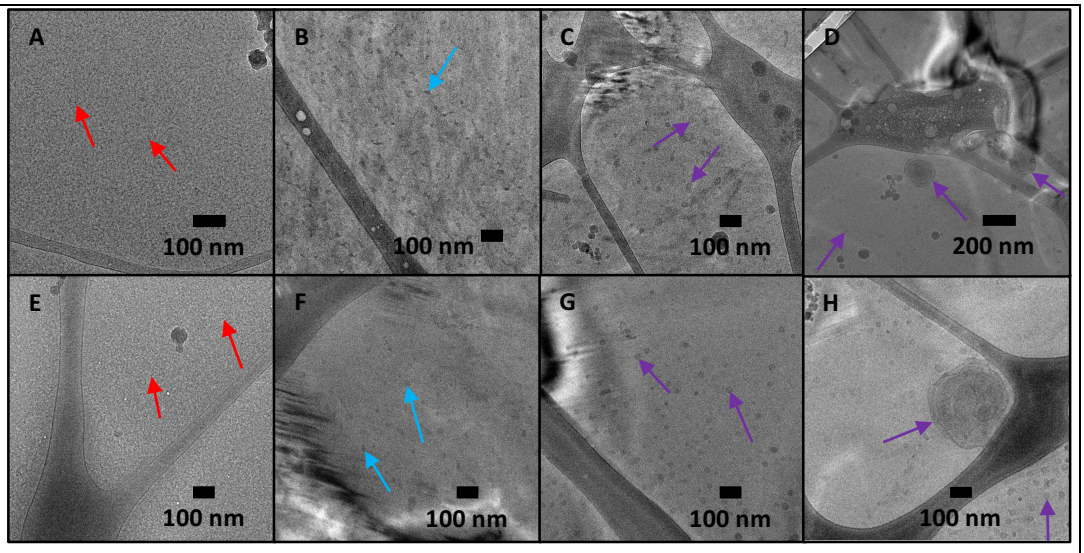

Figure 2. Summary of Micellar sample, vortex mixed for 15 seconds, cryo-frozen within 20 seconds using blotless method: A,B,C,D) no perfume; E,F,G,H) with perfume; A,E) 10x dilution; B,F) 20x dilution; C,D, G, H) 50x dilution.
Red arrows indicate micelles. Blue arrows indicate initial transition to small vesicles. Purple arrows indicate vesicles.

From these images, it can be seen that in general, as the dilution increases the size of the structures increases in the micellar system with no perfume. Also, when less dilute, there are no vesicles present in the system. Only micelles and wormlike micelles can be seen.

Figure 3 shows a graph indicating how the area of the vesicles present in the samples changes due to dilution.

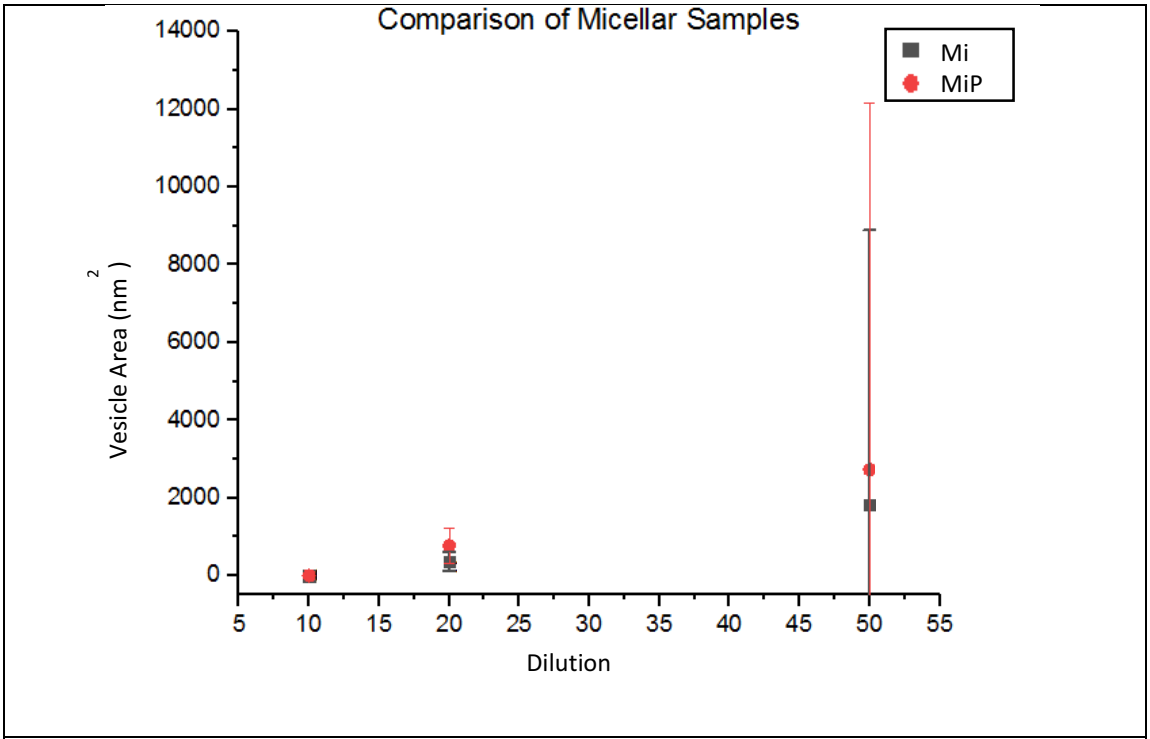

Figure 3. Graph showing how the area of the vesicles present changes due to dilution for the micellar samples with and without perfume at 10x, 20x, and 50x dilution. The black squares and error bars indicate area values (in nm^2) for Mi samples at the different dilutions, and the red circles and error bars indicate area values (in nm^2) for MiP samples at the different dilutions.

From this graph, the size increase due to dilution as seen in the Mi and MiP images from figure 2 can be confirmed. Figure 4 shows graphs of the micellar samples at 20 and 50 times dilution. When compared to figure 3 above, the overall size increase upon dilution can be confirmed, as well as the fact that there is more variability in the micellar samples at 50x dilution. It should be noted that for both the Mi and MiP samples at 50 times dilution, there are some larger values which were included in these graphs, which are highlighted in the appendix. These larger values also contribute to the large standard deviation seen figure 3.

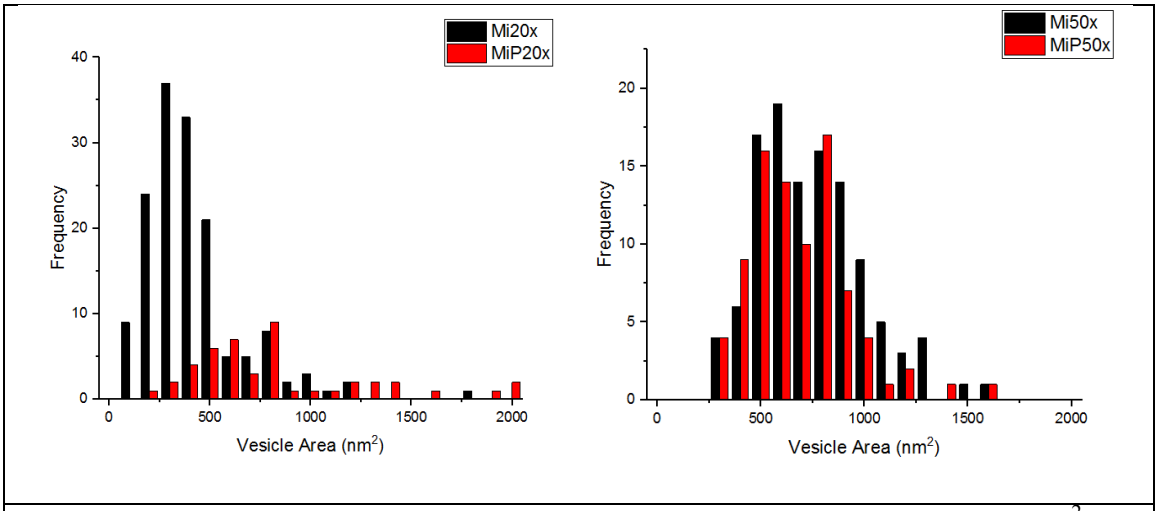

Figure 4. Graphs showing the areas of the vesicles present for each dilution in nm^2. The black bars indicate Mi samples and the red bars indicate MiP samples.

This is different from what is usually expected, as micelles would usually transform into monomers upon dilution, since the surfactant concentration in the system would be below the CMC [29]. However, in this case the systems were diluted with hard water, which is a salt solution. The addition of salts to micellar systems have been shown to increase the packing parameter by reducing headgroup repulsion, even at low surfactant concentrations, therefore inducing micelle/wormlike micelle formation [3, 30, 31]. As more salt solution is added to the system, the packing parameter continues to increase, and eventually vesicle formation becomes more favorable, as seen in the vesicle images in figure 2 [21, 32]. Initially, salt is absent from the original micellar samples, as shown in table 1, which further suggests that the reason for vesicle formation is the addition of salt via hard water. However, as the dilution increases and the surfactant ratio decreases, the addition of salt would have less of an impact and the system would follow the logical transition from vesicles to micelles and eventually to monomers.

It is known that the addition of perfume may alter the curvature and packing constraints of a system, depending on whether it acts as a co-surfactant and/or co-solvent,

therefore causing changes in the structures present [33-35]. It is more commonly assumed that perfume acts as a co-surfactant, allowing the formation of vesicles with more bilayers [33-35]. However, in the micellar samples, the perfume does not seem to have much of an effect. The only noticeable effect is that the standard deviation for the samples with perfume is larger than the standard deviation for the no perfume samples, meaning that there is a larger size distribution in the perfume samples. Given the large standard deviation overall, there is not a noticeable difference in the sizes of the structures found in the Mi and MiP samples.

The remaining figures show images of the lamellar systems with and without perfume at 10x, 20x, and 50x dilution.

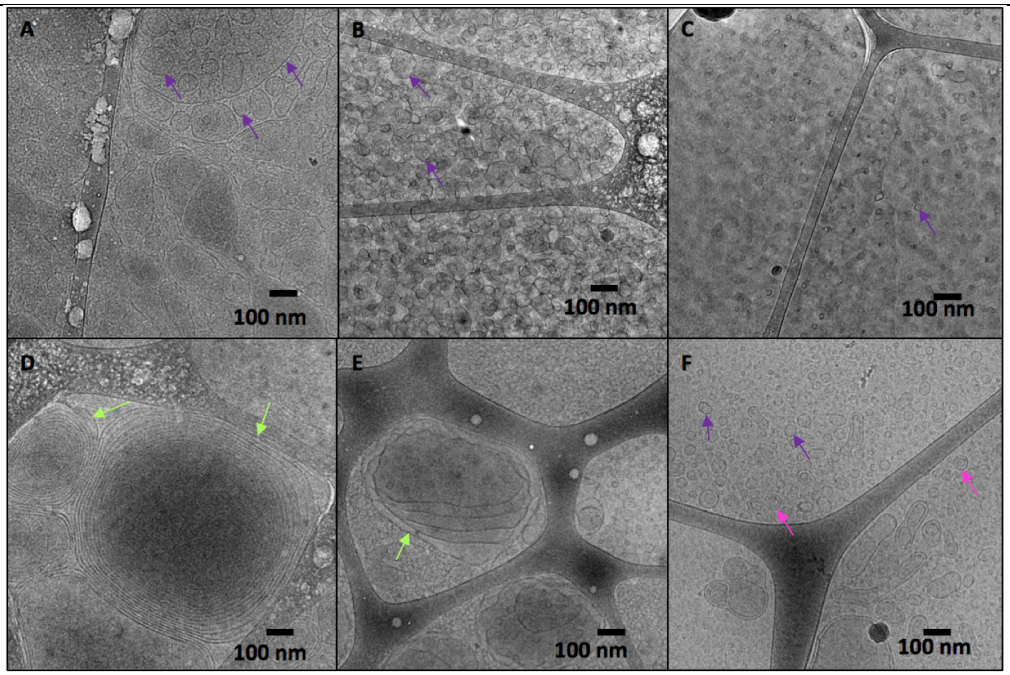

Figure 5. Summary of Lamellar sample, vortex mixed for 15 seconds, cryo-frozen within 20 seconds using blotless method: A,B,C) no perfume; D,E,F) with perfume; A,D) 10x dilution; B,E) 20x dilution; C,F) 50x dilution. Purple arrows indicate unilamellar vesicles. Green arrows indicate multilamellar vesicles. Pink arrows indicate bilamellar vesicles. As dilution increases, curvature increases, causing transformations from larger vesicles to smaller vesicles with less layers.

As a general trend, both lamellar systems (with and without perfume) show a decrease in vesicle size with increase in dilution ratio. This is quite different from the micellar samples which showed changes from wormlike micelles and micelles to vesicles. In lamellar systems, the addition of salt has less of an effect on the structural transformations, while the effects of perfume are more obvious. This can also be attributed to the fact that there was already some salt present in the original lamellar samples before the addition of hard water, as shown in Table 1. The only thing that salt may have an effect on is an increase in the lamellar repeat distance [36].

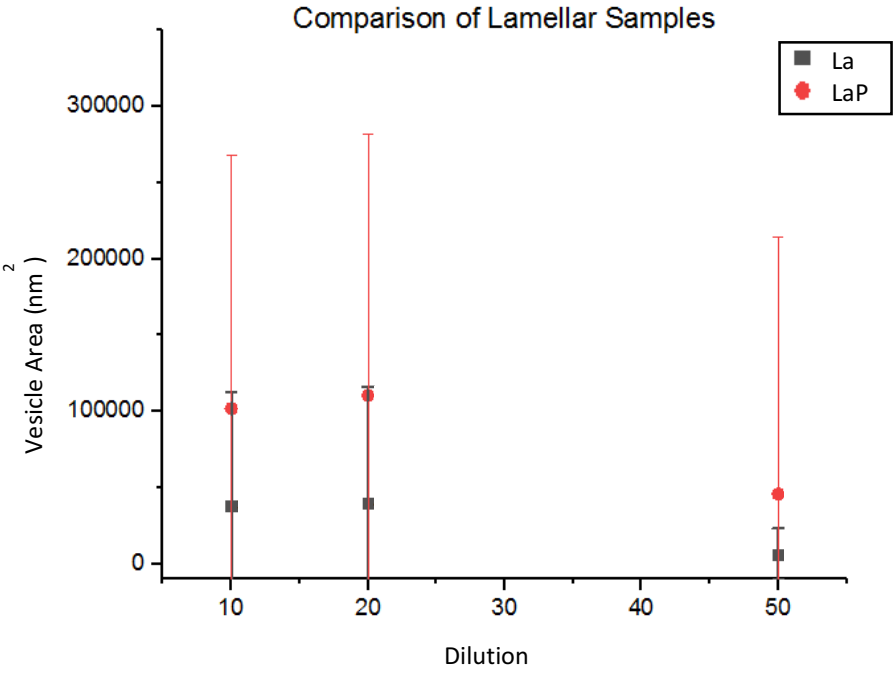

Figure 6. Graph showing how the area of the vesicles present changes due to dilution for the lamellar samples with and without perfume at 10x, 20x, and 50x dilution. The black squares and error bars indicate area values (in nm^2) for La samples at the different dilutions, and the red circles and error bars indicate area values (in nm^2) for LaP samples at the different dilutions.

Figure 6 shows a graph indicating how the area of the vesicles present in the samples changes as a function of dilution. However, like the micellar samples, the standard deviation is larger for the LaP samples, and smaller for the La samples, meaning that the size distribution is larger for the LaP samples. Given the large standard deviation, one might say that there is no change, however this is due to a smaller number of outliers present throughout the samples. Overall, it can be seen through the images that the area does decrease with an increase in dilution.

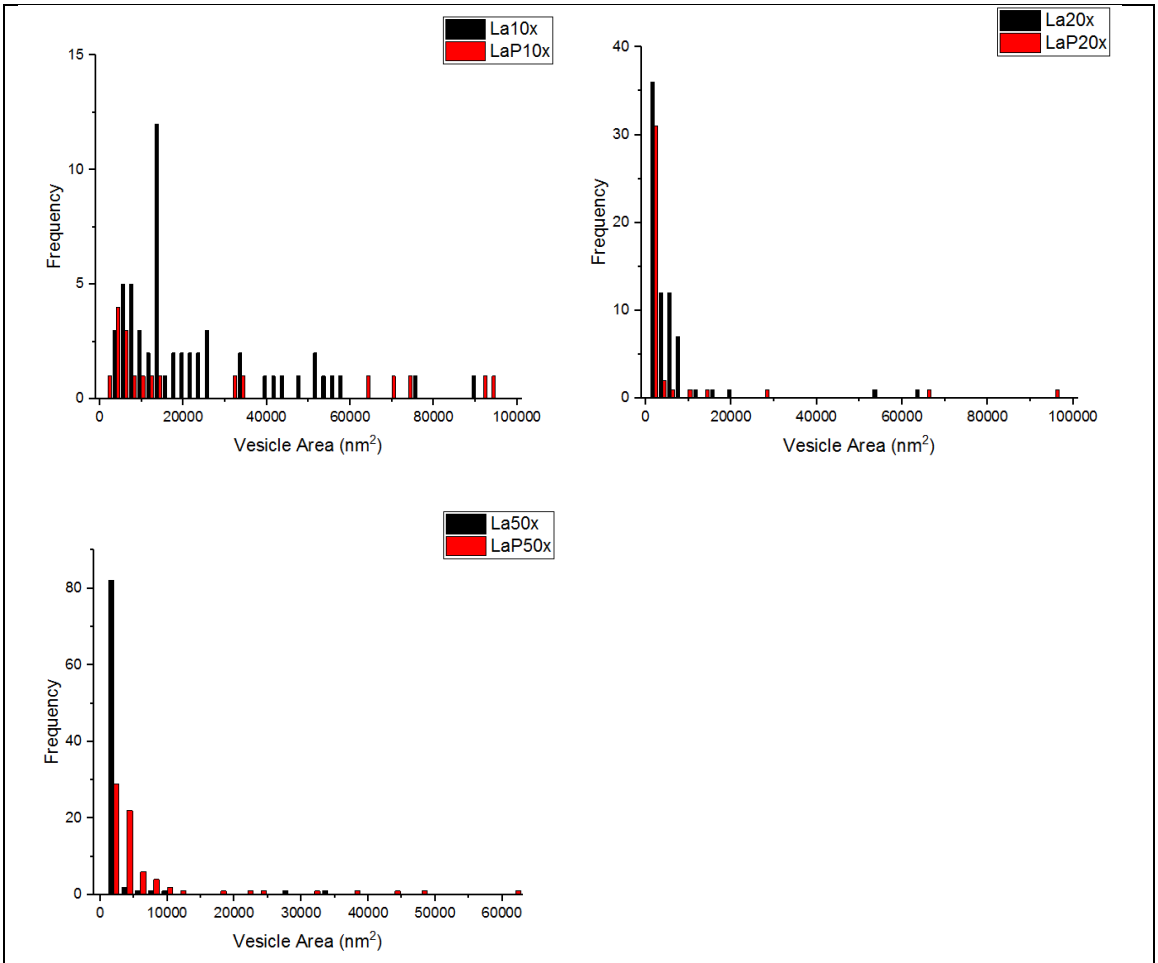

Figure 7. Graphs showing the areas of the vesicles present for each dilution in nm^2. The black bars indicate La samples and the red bars indicate LaP samples.

The general trend showing a decrease in size with dilution increase shown in the graph is in agreement with the visual results shown in figures 6 and 7. Another outcome that is initially surprising is that the average vesicle size at 20x dilution is slightly larger than the average vesicle size at 10 times dilution. However, upon closer inspection this makes sense for a few reasons. First, the variability for the samples at 20 times dilution are larger, meaning that the ranges of vesicle sizes are larger. Also, although the majority of the vesicles are smaller and have less bilayers at 20 times dilution, there are a few which are larger and contain many smaller vesicles within.

In aqueous solutions, surfactants often aggregate into structures, due to enthalpic or entropic driving forces [37, 38]. The curvature of this aggregate can change depending on many variables such as temperature, surfactant concentration, pH, as well as addition of electrolytes/salt, head group size, surfactant tail length, and number/types of surfactants present [39-41]. Structures formed in these systems depend on the curvature of these films, and in some instances these films form micelles by closing up [39]. Similarly, in systems with multiple surfactants present, surfactant bilayers may close up and form vesicles [39]. More specifically, the flexibility/rigidity of the film, which depends on the packing parameter, dictates what kind of aggregates are formed in the system; tail length and flexibility also have an effect on structures formed and on transitions that take place in mixed surfactant systems [30, 42-44].

Perfume seems to take on a co-surfactant role in the lamellar samples, due to the fact that the systems with perfume contain vesicles with many more layers than the ones found in the no perfume systems. By acting as a co-surfactant, the perfume would increase the surfactant efficiency by increasing the hydrophobicity of the surfactant, and

therefore increasing the packing parameter, causing vesicles to form more readily [34]. Although effects of shearing have been known to produce multilamellar vesicles in mixed surfactant systems, and are a factor in the structures present, the same shear was applied to the samples over the same timescale, therefore the increase in layer number from the no perfume sample to the sample with perfume can be directly attributed to the co-surfactant qualities of the perfume [45-49]. Also, since the amount of hard water added at each dilution is the same, salt cannot account for the difference in layers seen in the La and LaP samples.

Dilution expands the water layer, lowering the surfactant concentration present in the system. In order to maintain equilibrium, curvature must increase, causing the transition from larger vesicles to smaller unilamellar and bilamellar as seen in figure 5 [50, 51]. Therefore, a logical progression of expected structures observed with increasing dilution would be: multilamellar vesicles→unilamellar/bilamellar vesicles→micelles.

Since the micellar samples have a different formulation than the lamellar samples, the progression would be slightly different: wormlike micelle/micelle→unilamellar/bilamellar→ micelle, and eventually monomers. After dilution, the size of the structures would initially increase, and there would be a transition to vesicles, however upon further increase of the hydrophilic layer, the decrease in surfactant density would cause larger structures to break up and would transform into a more energetically stable micellar structure.

CHAPTER 4

CONCLUSION

As the dilution increases, initially micellar and lamellar systems seem to behave differently. Both micellar systems show an overall increase in the sizes of the nanostructures present, shown by the formation of larger, unilamellar vesicles from wormlike micelles/micelles. For lamellar samples, lower dilution ratios show tightly packed multilamellar vesicles, while higher dilution ratios show more dispersed vesicles with less bilayers. However, it has been predicted that both systems would eventually show transitions to from vesicles to micelles, and eventually monomers at even higher dilutions.

The effects of perfume on the nanostructures present in the samples were also considered, and it was found that the addition of perfume in lamellar samples caused more bilayers to form, though this did not always indicate a larger vesicles size. These effects indicated the role of perfume as a co-surfactant in the lamellar sample. In the micellar sample, the role of perfume was negligible. The mean area calculated for the samples with perfume was slightly larger than the no perfume sample, but due to the large standard deviation, it can't be said that perfume made a meaningful difference in the formulation.

Suggestions for future work

In order to see nanostructural transformations at smaller dilution increments, future experiments with more dilution ratios in between those used in this study (such as 15x, 30x, and 40x) should be tested. Also, in order to achieve a better understanding of what

the final nanostructures present are at higher dilutions, dilutions such as 120x, 150x, and 200x should be tested.

Some other suggestions for future work would be to use methods such as DLS in order to investigate the sizes of the nanostructures present more closely. The values obtained through DLS could then be compared to the values to the values obtained through cryo-TEM in this study.

APPENDIX

Mi 10x	Vesicle Area (nm^2)	MiP 10x	Vesicle Area (nm^2)
	0		0

Mi 20x	Vesicle Area (nm^2)	MiP 20x	Vesicle Area (nm^2)
	42.32532772		183.87789
	44.81710942		211.189171
	49.78909449		263.3670509
	62.23935184		300.6419543
	79.6748612		318.0353066
	89.61795482		360.2862681
	93.22756703		362.7801743
	99.57874818		422.4047888
	99.57874818		422.4047888
	102.0703453		459.6565245
	113.3802556		459.6565245
	123.7416044		482.0389679
	123.7416044		496.9400445
	143.5420081		509.3441833
	150.9617705		516.8117082
	160.8757322		526.7715779
	160.8757322		549.1341884
	161.8213296		576.4637668
	161.8213296		598.8052658
	161.8213296		598.8052658
	169.3013109		636.0608005
	171.3136871		648.5034402
	179.2447069		680.8077613
	179.2447069		715.6031469
	181.4106426		715.6031469
	181.745018		720.5427485
	181.745018		720.5427485
	184.2385881		720.5427485
	184.2385881		725.5470817
	186.4343988		740.4228214
	186.4343988		777.7287692
	199.1813921		787.6461489
	199.1813921		807.518294
	200.4591964		966.5711107
	201.5648988		1046.060052

	204.1398141 210.3657219 210.3657219 211.6272826 211.6272826 211.6272826 214.1617185 222.7540624 224.0787149 224.0787149 240.0611026 242.5390652 243.9765764 247.4773913 247.4773913 248.9574074 257.3895936 258.9274346 263.885065 271.36586 279.6621433 279.6621433 279.6621433 279.6621433 279.6621433 279.6621433 281.3244982 281.3244982 281.3244982 281.3244982 281.3244982 288.8058084 288.8058084 289.559339 289.559339 301.256921 301.256921 301.9341102 303.7230713 309.371014		1195.14202 1195.14202 1217.488406 1292.0692 1316.907499 1364.083948 1552.909006 1813.857619 1900.779814 1928.155871

	309.371014 311.213108 311.213108 311.213108 318.6678035 321.7443267 322.4759792 323.6547292 323.6547292 338.5868518 338.5868518 338.5868518 339.0762451 339.0762451 341.070086 358.8746343 358.8746343 361.3299657 363.4894713 363.4894713 366.2996629 367.8277846 367.8277846 368.7461844 368.7461844 378.64819 388.5765652 390.8859751 400.9369942 403.3183882 403.3183882 405.8853584 405.8853584 405.8853584 405.8853584 408.1381372 413.2026618 420.7307472 423.2430561 428.1433971		

	428.2901095 430.7144922 445.479296 447.9517828 448.1393712 457.8722263 480.1340231 494.9664174 499.9474786 524.6989161 539.5403425 556.845043 574.1680323 577.5707541 606.3322712 614.7409827 618.746588 659.7456798 689.6231174 717.7383893 717.7383893 726.9800721 732.5822426 754.8650275 761.8448775 770.9224113 784.5650413 834.0241814 890.9633428 915.7344514 949.8371151 975.1312714 1051.858012 1133.518124 1133.518124 1725.802018		

Mi 50x	Vesicle Area (nm^2)	MiP 50x	Vesicle Area (nm^2)
	222.595368 281.5921218		226.4196413 226.4196413

	289.3784021		254.4124594
	289.3784021		280.7599328
	354.2892796		323.0173
	365.0455901		325.6347525
	378.4067986		337.9022948
	378.4067986		348.541135
	391.5871472		370.2111853
	396.230641		370.2111853
	426.7874991		379.0621828
	429.5749148		390.080404
	429.5749148		397.5371375
	431.8187463		407.49385
	431.8187463		419.8949728
	436.2869213		429.9423555
	436.2869213		432.4819774
	439.9969851		442.2678374
	439.9969851		442.2678374
	442.8644385		447.2393049
	445.1800656		457.910154
	445.1800656		459.6565245
	445.1800656		460.4548857
	457.5688616		470.6274192
	457.5688616		470.6274192
	469.4361768		470.6274192
	471.8971748		479.5516307
	500.4628168		486.9938289
	510.3847636		490.9916689
	514.7989683		501.8912927
	518.1826144		501.8912927
	518.1826144		508.7843106
	520.8489689		508.7843106
	535.8823827		509.3441833
	540.3228669		513.8744266
	543.1281269		521.5368653
	549.9652025		549.1341884
	553.587425		559.0640056
	556.4686762		559.0640056
	563.1786155		562.2115869
	571.961654		562.2115869
	575.7405415		568.9982368

	578.7214417		572.3856277
	578.7214417		608.7350988
	598.371616		608.7350988
	598.371616		608.7350988
	637.9844267		621.1738649
	642.1547614		658.426075
	642.1547614		661.4312314
	642.3793577		680.8077613
	642.3793577		684.327099
	655.5638995		688.2739486
	659.882266		697.0437611
	663.3471663		714.8447162
	663.3471663		715.6031469
	673.1523377		718.070824
	677.6204309		720.5427485
	681.1315314		720.5427485
	690.7872542		720.5427485
	695.3133993		725.5470817
	703.9867122		732.6781931
	703.9867122		735.4634914
	708.6030062		737.772562
	712.2879813		757.8385175
	712.2879813		757.8385175
	717.4535065		777.7287692
	721.2089923		777.7287692
	726.3111673		796.2753633
	726.3111673		796.2753633
	748.4505991		796.2753633
	752.8697369		805.0521681
	752.8697369		807.518294
	756.8141973		814.0793532
	788.3427185		826.7713875
	796.3753979		839.8184021
	797.1759008		839.8184021
	801.5858549		859.7103581
	819.347314		906.905826
	823.6146084		916.8611624
	849.1928549		919.3316166
	849.1928549		989.6307527
	859.1907387		1075.849495

	859.1907387		1124.465738
	859.1907387		1144.764699
	863.6645991		1383.991325
	868.0456318		1562.843121
	876.9984098		15509.47401
	888.7426766		27562.78479
	894.6175955		45181.64971
	894.6175955		48501.27477
	901.9485365		57058.48246
	915.1445459		
	943.7833045		
	978.7876988		
	978.7876988		
	978.7876988		
	978.7876988		
	989.9653323		
	996.5009375		
	1007.553916		
	1036.337294		
	1073.583356		
	1085.054707		
	1085.054707		
	1107.177453		
	1151.491175		
	1161.919904		
	1210.879941		
	1219.777761		
	1244.477241		
	1291.050017		
	1439.328906		
	1598.783145		
	7783.29847		
	29938.63035		
	30750.33057		
	64908.13204		

La 10x	Vesicle Area (nm^2)	LaP 10x	Vesicle Area (nm^2)
	2089.630009		1053.525733
	2594.013761		2149.277687
	3349.316181		2370.389752

	4021.668495		2516.95929
	4325.868017		3702.197021
	4462.508966		4119.598545
	4676.240436		4315.848234
	5153.251822		4633.914622
	6147.12604		6452.809448
	7238.983476		8075.113946
	7255.279501		10460.36065
	7575.788397		12674.27104
	7754.708842		30067.26877
	8301.254		33538.51951
	8525.933824		62514.27271
	9504.00894		68222.36667
	10080.46815		72743.41471
	11792.80942		90645.21763
	12339.87727		93841.65773
	12584.83458		119887.0455
	12584.83458		194128.4685
	12587.41961		246902.0286
	12951.13605		314160.7237
	13191.0625		510115.3117
	13337.22161		646879.4385
	13390.08524		
	13680.63101		
	13698.0509		
	13743.10359		
	13906.909		
	14808.78808		
	16888.64416		
	17223.8255		
	18014.04449		
	18393.31741		
	20675.14602		
	21529.93342		
	23281.44249		
	23736.09621		
	24966.54615		
	25760.85984		
	25780.77744		
	33027.292		

	33710.45205 38217.08737 40731.13944 43198.45064 46131.86552 50102.99954 51226.0484 53991.50597 54625.12998 57606.80638 74343.54147 88585.46777 108629.282 155405.4709 364415.7015 440871.5595		

La 20x	Vesicle Area (nm^2)	LaP 20x	Vesicle Area (nm^2)
	407.49385		248.4822046
	422.4047888		310.5880568
	459.6565245		318.0353066
	479.5516307		340.4157236
	503.8786642		360.2862681
	549.1341884		370.2111853
	568.9982368		422.4047888
	651.0787914		449.7166644
	718.070824		606.2449852
	720.5427485		606.2449852
	757.8385175		658.426075
	777.7287692		725.5470817
	777.7287692		735.4634914
	807.518294		757.8385175
	839.8184021		787.6461489
	906.905826		805.0521681
	940.4646761		807.518294
	970.3771023		827.3830744
	974.0246139		837.3546898
	977.8452375		974.0246139
	1046.060052		974.0246139
	1080.155915		978.9540626

	1205.089213 1229.826742 1277.140371 1322.12265 1396.415595 1403.843677 1559.061627 1589.017878 1629.9754 1629.9754 1672.178792 1674.716543 1681.323701 1711.986839 2089.630009 2099.60775 2397.737348 2516.95929 2633.795263 2753.002795 2818.863344 2886.168919 2946.855155 3508.41357 3888.578953 3968.00764 4047.562743 4238.877317 4405.385663 4810.3942 4942.083091 5014.115237 5260.042854 5399.271172 5588.047064 5588.047064 5749.517937 5916.014886 6005.51025 6087.515545		1053.525733 1056.000993 1098.231077 1137.998133 1224.983198 1224.983198 1354.151727 1441.145072 1503.232451 2367.887862 2516.95929 4258.749103 9036.787149 12920.49417 27217.52461 64048.05115 94001.35767 161455.5257 216320.3589 216665.909 1043219.071

	6124.772747		
	6298.688917		
	6348.584351		
	6899.968617		
	7195.616981		
	11292.96367		
	14111.6618		
	18371.68924		
	52627.13268		
	62758.69456		
	121678.9654		

La 50x	Vesicle Area (nm^2)	LaP 50x	Vesicle Area (nm^2)
	89.09855295		211.189171
	178.2021065		323.0173
	184.2385881		449.7166644
	210.3657219		541.6420844
	210.3657219		549.0926542
	220.2743468		613.2038289
	247.4773913		658.8354662
	263.885065		732.2944287
	309.371014		793.1274898
	321.7443267		793.1274898
	321.7443267		1013.582857
	323.6547292		1054.101116
	338.5868518		1097.174041
	360.9931241		1127.618041
	361.3299657		1228.956684
	363.4894713		1279.675322
	368.7461844		1279.675322
	400.9369942		1388.610895
	420.7307472		1391.121885
	420.7307472		1411.424638
	445.479296		1455.986145
	445.479296		1464.655935
	447.9517828		1552.909006
	447.9517828		1583.723215
	450.6192188		1621.756479
	460.5689938		1654.684705
	460.5689938		1707.882411

	460.5689938		1745.888206
	485.0791091		1890.361959
	487.5415844		2108.225519
	507.3460518		2141.150407
	510.3847636		2153.881754
	514.7587535		2283.101454
	546.9350397		2308.23882
	546.9350397		2354.022086
	550.2146292		2354.022086
	550.2146292		2447.375827
	556.845043		2452.903099
	560.1541666		2579.590081
	562.631932		2627.704251
	603.8470822		2648.643139
	607.4675611		2725.63644
	609.9601817		2882.170994
	618.7024997		2894.649869
	618.7024997		3167.420492
	637.3578109		3180.40171
	639.8212869		3259.8584
	643.457967		3296.696966
	655.8362191		3309.532298
	659.7456798		3746.871451
	677.1591195		3960.530573
	677.1591195		4534.549905
	689.6231174		5131.263216
	715.2238813		5194.559267
	726.9800721		5478.615889
	732.5822426		5667.560934
	736.9062364		5749.517937
	774.6178078		6580.724994
	774.6178078		6631.290085
	774.6178078		6842.814706
	784.5153955		6943.026959
	784.5153955		8777.675917
	806.6119319		9471.55145
	809.1308609		10375.8745
	816.609906		16580.02732
	863.7166891		20641.51837
	975.0759236		22351.92326

	989.9653323 1120.309081 1125.297993 1244.789896 1274.671214 1294.618917 1356.827239 1366.769249 1443.972496 1458.895782 1526.134315 1645.61263 1692.899296 1843.797826 1854.773696 2519.449743 2990.021333 5599.182326 6555.156254 9923.591274 26927.64037 33181.76545 241883.912		31908.55956 37839.30072 43342.24259 47321.10526 60532.45006 110106.9972 128041.7271 212890.657

BIBLIOGRAPHY

1. Bujak, T., T. Wasilewski, and Z. Nizioł-Łukaszewska, *Role of macromolecules in the safety of use of body wash cosmetics.* Colloids and Surfaces B: Biointerfaces, 2015. **135**: p. 497-503.

2. Regan, J., L.-M. Mollica, and K.P. Ananthapadmanabhan, *A Novel Glycinate-based Body Wash: Clinical Investigation Into Ultra-mildness, Effective Conditioning, and Improved Consumer Benefits.* The Journal of clinical and aesthetic dermatology, 2013. **6**(6): p. 23.

3. Tang, X., et al., *Multiscale Modeling of the Effects of Salt and Perfume Raw Materials on the Rheological Properties of Commercial Threadlike Micellar Solutions.* The Journal of Physical Chemistry B, 2017. **121**(11).

4. Mohanty, A., T. Patra, and J. Dey, *Salt-induced vesicle to micelle transition in aqueous solution of sodium N-(4-n-octyloxybenzoyl)-L-valinate.* The journal of physical chemistry. B, 2007. **111**(25): p. 7155.

5. Kusano, T., et al., *Structural and rheological studies on growth of salt-free wormlike micelles formed by star-type trimeric surfactants.* Langmuir : the ACS journal of surfaces and colloids, 2012. **28**(49): p. 16798.

6. Jiang, L., et al., *Bile salt-induced vesicle-to-micelle transition in catanionic surfactant systems: steric and electrostatic interactions.* Langmuir : the ACS journal of surfaces and colloids, 2008. **24**(9): p. 4600.

7. Uddin, M.H., N. Kanei, and H. Kunieda, *Solubilization and Emulsification of Perfume in Discontinuous Cubic Phase.* Langmuir, 2000. **16**(17): p. 6891-6897.
8. Mendes, E., et al., *A Small-Angle Neutron Scattering Study of a Shear-Induced Vesicle to Micelle Transition in Surfactant Mixtures.* The Journal of Physical Chemistry B, 1998. **102**(2): p. 338-343.

9. Wasilewski, T. and T. Bujak, *Effect of the Type of Nonionic Surfactant on the Manufacture and Properties of Hand Dishwashing Liquids in the Coacervate Form.* Industrial & Engineering Chemistry Research, 2014. **53**(34): p. 13356-13361.

10. Baruah, A., et al., *Phase Behavior and Thermodynamic and Rheological Properties of Single- (SDS) and Mixed-Surfactant (SDS + CAPB)-Based Fluids with 3-Methylbutan-1-ol as the Cosurfactant and Pine Oil as the Organic Phase.* Industrial & Engineering Chemistry Research, 2014. **53**(51): p. 19765-19774.

11. Oliver, R.C., et al., *Tuning micelle dimensions and properties with binary surfactant mixtures.* Langmuir : the ACS journal of surfaces and colloids, 2014. **30**(44): p. 13353.

12. Georgieva, G.S., et al., *Synergistic Growth of Giant Wormlike Micelles in Ternary Mixed Surfactant Solutions: Effect of Octanoic Acid.* Langmuir : the ACS journal of surfaces and colloids, 2016. **32**(48): p. 12885.

13. Ruiz, M.O., et al., *Equilibrium Distribution Model of Betaine between Surfactant Micelles and Water: Application to a Micellar-Enhanced Ultrafiltration Process.* Industrial & Engineering Chemistry Research, 2010. **49**(14): p. 6578-6586.

14. Joo, K.-M., et al., *Relationship of ceramide–, and free fatty acid–cholesterol ratios in the stratum corneum with skin barrier function of normal, atopic dermatitis lesional and non-lesional skins*. 2015. p. 71-74.

15. Pham, Q.D., et al., *Chemical penetration enhancers in stratum corneum — Relation between molecular effects and barrier function.* Journal of Controlled Release, 2016. **232**: p. 175-187.

16. Smeden, J., et al., *The importance of free fatty acid chain length for the skin barrier function in atopic eczema patients.* Experimental Dermatology, 2014. **23**(1): p. 45-52.

17. Simpson, E.L., et al., *Emollient enhancement of the skin barrier from birth offers effective atopic dermatitis prevention.* The Journal of Allergy and Clinical Immunology, 2014. **134**(4): p. 818-823.

18. Lemery, E., et al., *Surfactants have multi-fold effects on skin barrier function.* European Journal of Dermatology, 2015. **25**(5): p. 424-435.

19. Telofski, L.S., et al., *The Infant Skin Barrier: Can We Preserve, Protect, and Enhance the Barrier?* Dermatology Research and Practice, 2012. **2012**.

20. Walters, R.M., et al., *Cleansing Formulations That Respect Skin Barrier Integrity.* Dermatology Research and Practice, 2012. **2012**.

21. Renoncourt, A., et al., *Specific Alkali Cation Effects in the Transition from Micelles to Vesicles through Salt Addition.* Langmuir, 2007. **23**(5): p. 2376-2381.

22. Dey, D., et al., *Development of hard water sensor using fluorescence resonance energy transfer.* Sensors & Actuators: B. Chemical, 2013. **184**: p. 268-273.

23. Tokatli, C., et al., *Statistical approaches to evaluate the aquatic ecosystem qualities of a significant mining area: Emet stream basin (Turkey).* Environmental Earth Sciences, 2014. **71**(5): p. 2185-2197.

24. WHO *Hardness in Drinking-water*. 2011.

25. *LabTech; Hard Water Contamination In Homes Costs Unseen Thousands*. 2015: Atlanta. p. 122.

26. *sodium 2-[2-[2-(tridecyloxy)ethoxy]ethoxy]ethyl sulphate CAS#: 25446-78-0*. 2017; Available from: http://www.chemicalbook.com/ProductChemicalPropertiesCB1885437_EN.htm.

27. Pubchem. *Cocamidopropyl betaine*. 2017; Available from: https://www.ncbi.nlm.nih.gov/pubmed/.

28. Lee, J., et al., *Shear free and blotless cryo-TEM imaging: a new method for probing early evolution of nanostructures.* Langmuir : the ACS journal of surfaces and colloids, 2012. **28**(9): p. 4043.

29. Mukerjee, P., *Critical micelle concentrations of aqueous surfactant systems*, ed. K.J. Mysels and S. United States. National Bureau of. 1971, Washington, D.C.: Washington : U.S. National Bureau of Standards; for sale by the Supt. of Docs., U.S. Govt. Print. Off.

30. Nagarajan, R., *Molecular Packing Parameter and Surfactant Self-Assembly: The Neglected Role of the Surfactant Tail †.* Langmuir, 2002. **18**(1): p. 31-38.

31. Raghavan, S.R., H. Edlund, and E.W. Kaler, *Cloud-Point Phenomena in Wormlike Micellar Systems Containing Cationic Surfactant and Salt.* Langmuir, 2002. **18**(4): p. 1056-1064.

32. Lu, H., L. Wang, and Z. Huang, *Unusual pH-responsive fluid based on a simple tertiary amine surfactant: the formation of vesicles and wormlike micelles.* RSC Adv., 2014. **4**(93): p. 51519-51527.

33. Bradbury, R., et al., *Impact of model perfume molecules on the self-assembly of anionic surfactant sodium dodecyl 6-benzene sulfonate.* Langmuir : the ACS journal of surfaces and colloids, 2013. **29**(10): p. 3234.

34. Tchakalova, V., et al., *Solubilization and interfacial curvature in microemulsions: II. Surfactant efficiency and PIT.* Colloids and Surfaces A: Physicochemical and Engineering Aspects, 2008. **331**(1): p. 40-47.

35. Tchakalova, V., et al., *Solubilization and interfacial curvature in microemulsions: I. Interfacial expansion and co-extraction of oil.* Colloids and Surfaces A: Physicochemical and Engineering Aspects, 2008. **331**(1): p. 31-39.

36. Hishida, M., Y. Yamamura, and K. Saito, *Salt effects on lamellar repeat distance depending on head groups of neutrally charged lipids.* Langmuir : the ACS journal of surfaces and colloids, 2014. **30**(35): p. 10583.

37. Strey, R., *Phase behavior and interfacial curvature in water-oil-surfactant systems.* Current Opinion in Colloid & Interface Science, 1996. **1**(3): p. 402-410.

38. Balogh, J., et al., *Effects of oil on the curvature elastic properties of nonionic surfactant films: thermodynamics of balanced microemulsions.* Physical review. E, Statistical, nonlinear, and soft matter physics, 2006. **73**(4 Pt 1): p. 041506.

39. Bergström, L.M., *Model calculations of the spontaneous curvature, mean and Gaussian bending constants for a thermodynamically open surfactant film.* Journal of Colloid And Interface Science, 2006. **293**(1): p. 181-193.

40. Balogh, J. and U. Olsson, *Dependence on Oil Chain-Length of the Curvature Elastic Properties of Nonionic Surfactant Films: Droplet Growth from Spheres to a Bicontinuous Network.* Journal of Dispersion Science and Technology, 2007. **28**(2): p. 223-230.

41. Genç, R., M. Ortiz, and C.K. Sullivan, *Curvature-tuned preparation of nanoliposomes.* Langmuir : the ACS journal of surfaces and colloids, 2009. **25**(21): p. 12604.

42. Bergström, L.M., *Bending elasticity of charged surfactant layers: the effect of layer thickness.* Langmuir : the ACS journal of surfaces and colloids, 2006. **22**(8): p. 3678.

43. Szleifer, I., et al., *Molecular theory of curvature elasticity in surfactant films.* The Journal of Chemical Physics, 1990. **92**(11): p. 6800-6817.

44. Cantor, R.S., *Statistical thermodynamics of curvature elasticity in surfactant monolayer films: A molecular approach.* The Journal of Chemical Physics, 1993. **99**(9): p. 7124-7149.

45. Medronho, B., et al., *Shear-induced transitions between a planar lamellar phase and multilamellar vesicles: continuous versus discontinuous transformation.* Langmuir : the ACS journal of surfaces and colloids, 2008. **24**(13): p. 6480.

46. Genty, M., et al., *Characterization of a complex dispersion of multilamellar vesicles.* Kolloid-Zeitschrift und Zeitschrift für Polymere., 2003. **282**(1): p. 32-40.

47. Courbin, L., et al., *Instability of a lamellar phase under shear flow: formation of multilamellar vesicles.* Physical review letters, 2002. **89**(14): p. 148305.

48. Lu, C.Y.D., *Sizes of multilamellar vesicles in shear.* Physical review letters, 2012. **109**(12): p. 128304.

49. Youssry, M., et al., *Effect of shear on vesicle and lamellar phases of DDAB/lecithin ternary systems.* Journal of Colloid And Interface Science, 2011. **358**(2): p. 506-512.

50. Bagdassarian, C.K., et al., *Curvature defects in lamellar phases of amphiphile–water systems.* The Journal of Chemical Physics, 1991. **94**(4): p. 3030-3041.

51. Chen, Y.L., Z. Xu, and J. Israelachvili, *Structure and interactions of surfactant-covered surfaces in nonaqueous (oil-surfactant-water) media.* Langmuir, 1992. **8**(12): p. 2966-2975.